IMPROVING FEW-SHOT VISUAL CLASSIFICATION WITH UNLABELLED EXAMPLES

Peyman Bateni[*]
University of British Columbia, Inverted AI
Vancouver, BC
pbateni@cs.ubc.ca

Jarred Barber[*]
Amazon[†]
Cambridge, MA
jarred.barber@gmail.com

Jan-Willem van de Meent
Northeastern University
Boston, MA
j.vandemeent@northeastern.edu

Frank Wood
University of British Columbia, Inverted AI
Vancouver, BC
fwood@cs.ubc.ca

ABSTRACT

We propose a transductive meta-learning method that uses unlabelled instances to improve few-shot image classification performance. Our approach combines a regularized Mahalanobis-distance-based soft k-means clustering procedure with a modified state of the art neural adaptive feature extractor to achieve improved test-time classification accuracy using unlabelled data. We evaluate our method on transductive few-shot learning tasks, in which the goal is to jointly predict labels for query (test) examples given a set of support (training) examples. We achieve new state of the art performance on Meta-Dataset, and produce competitive results on mini- and tiered-ImageNet benchmarks.

1 INTRODUCTION

Deep learning has revolutionized visual classification, enabled in part by the development of large and diverse sets of curated training data (Szegedy et al., 2014; He et al., 2015; Krizhevsky et al., 2017; Simonyan & Zisserman, 2014; Sornam et al., 2017). However, in many image classification settings, millions of labelled examples are not available; therefore, techniques that can achieve sufficient classification performance with few labels are required. This has motivated research on few-shot learning (Feyjie et al., 2020; Wang & Yao, 2019; Wang et al., 2019; Bellet et al., 2013), which seeks to develop methods for developing classifiers with much smaller datasets. Given a few labelled "support" images per class, a few-shot image classifier is expected to produce labels for a given set of unlabelled "query" images. Typical approaches to few-shot learning adapt a base classifier network to a new support set through various means, such as learning new class embeddings (Snell et al., 2017; Vinyals et al., 2016; Sung et al., 2018), amortized (Requeima et al., 2019; Oreshkin et al., 2018) or iterative (Yosinski et al., 2014) partial adaptation of the feature extractor, and complete fine-tuning of the entire network end-to-end (Ravi & Larochelle, 2017; Finn et al., 2017).

In addition to the standard fully supervised setting, techniques have been developed to exploit additional unlabeled support data (semi-supervision) (Ren et al., 2018) as well as information present in the query set (transduction) (Liu et al., 2018; Kim et al., 2019). In our work, we focus on the transductive paradigm, where the entire query set is labeled at the same time. This allows us to exploit the additional unlabeled data, with the hopes of improving classification performance. Existing transductive few-shot classifiers rely on label propagation from labelled to unlabelled examples in the feature space through either k-means clustering with Euclidean distance (Ren et al., 2018) or message passing in graph convolutional networks (Liu et al., 2018; Kim et al., 2019).

Since few-shot learning requires handling a varying number of classes, an important architectural choice is the final feature to class mapping. Previous methods have used the Euclidean distance

[*] Authors contributed equally.

[†] Work performed while at Charles River Analytics

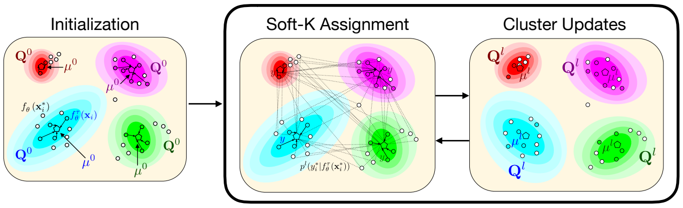
Initialization
Soft-K Assignment
Cluster Updates
$\mathbf{Q}^0$
μ^0
$f_\theta(\mathbf{x}_i^*)$
$f_\theta^\tau(\mathbf{x}_i)$
y
$p^l(y_i^*|f_\theta^\tau(\mathbf{x}_i^*))$
$\mathbf{Q}^l$
μ^l

Figure 1: Soft k-means Mahalanobis-distance based clustering method used in Transductive CNAPS. First, cluster parameters are initialized using the support examples. Then, during cluster update iterations, query examples are assigned class probabilities as soft labels and subsequently, both soft-labelled query examples and labelled support examples are used to estimate new cluster parameters.

(Ren et al., 2018), the absolute difference (Koch et al., 2015), cosine similarity (Vinyals et al., 2016), linear classification (Finn et al., 2017; Requeima et al., 2019) or additional neural network layers (Kim et al., 2019; Sung et al., 2018). Bateni et al. (2020) improved these results by using a class-adaptive Mahalanobis metric. Their method, Simple CNAPS, uses a conditional neural-adaptive feature extractor, along with a regularized Mahalanobis-distance-based classifier. This modification to CNAPS (Requeima et al., 2019) achieves improved performance on the Meta-Dataset benchmark (Triantafillou et al., 2019), only recently surpassed by SUR (Dvornik et al., 2020) and URT (Liu et al., 2020). However, performance suffers in the regime where there are five or fewer support examples available per class.

Motivated by these observations, we explore the use of unlabelled examples through transductive learning within the same framework as Simple CNAPS. Our contributions are as follows. **(1)** We propose a transductive few-shot learner, namely Transductive CNAPS, that extends Simple CNAPS with a transductive two-step task encoder, as well as an iterative soft k-means procedure for refining class parameter estimates (mean and covariance) using both labelled and unlabelled examples. **(2)** We demonstrate the efficacy of our approach by achieving new state of the art performance on Meta-Dataset (Triantafillou et al., 2019). **(3)** When deployed with a CIFAR100 pre-trained feature extractor, Transductive CNAPS achieves comparable performance on mini-ImageNet (Snell et al., 2017) and tiered-Imagenet (Ren et al., 2018), relative to other transductive methods. **(4)** When an ImageNet (Russakovsky et al., 2015) pre-trained feature extractor is employed on the same benchmarks, Transductive CNAPS outperforms other ImageNet-pretrained approaches such as CNAPS (Requeima et al., 2019) and Simple CNAPS with significant margins.

2 Related work

2.1 Few-Shot Learning using Labelled Data

Early work on few-shot visual classification has focused on improving classification accuracy through the use of better classification metrics with a meta-learned non-adaptive feature extractor. Matching networks (Vinyals et al., 2016) use cosine similarities over feature vectors produced by independently learned feature extractors. Siamese networks (Koch et al., 2015) classify query images based on the nearest support example in feature space, under the L_1 metric. Relation networks (Sung et al., 2018) and variants (Kim et al., 2019; Satorras & Estrach, 2018) learn their own similarity metric, parameterised through a Multi-Layer Perceptron. More recently, Prototypical Networks (Snell et al., 2017) learn a shared feature extractor that is used to produce class means in a feature space where the Euclidean distance is used for classification.

Other work has focused on adapting the feature extractor for new tasks. Transfer learning by fine-tuning pre-trained visual classifiers (Yosinski et al., 2014) was an early approach that proved limited in success due to issues arising from over-fitting. MAML (Finn et al., 2017) and its variants (Mishra et al., 2017; Nichol et al., 2018; Ravi & Larochelle, 2017) learn meta-parameters that allow fast task-adaptation with only a few gradient updates. Work has also been done on partial adaptation of feature extractors using conditional neural adaptive processes (Oreshkin et al., 2018; Garnelo et al., 2018; Requeima et al., 2019; Bateni et al., 2020). These methods rely on channel-wise adaptation of pre-trained convolutional layers by adjusting parameters of FiLM layers (Perez et al., 2018) inserted throughout the network. Our work builds on the most recent of these neural adaptive approaches, specifically Simple CNAPS (Bateni et al., 2020). SUR (Dvornik et al., 2020) and URT

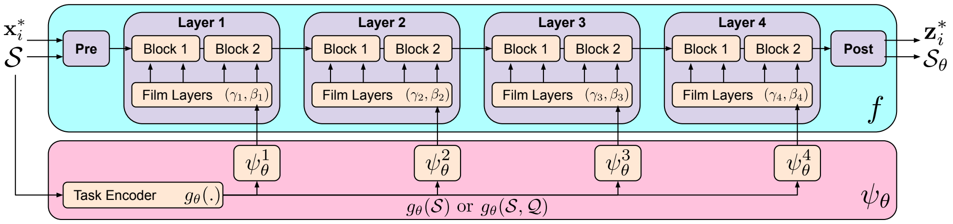
$\mathbf{x}_i^*$
$\mathcal{S}$
Pre
Layer 1
Layer 2
Layer 3
Layer 4
Block 1
Block 2
Film Layers (γ_1, β_1)
Film Layers (γ_2, β_2)
Film Layers (γ_3, β_3)
Film Layers (γ_4, β_4)
Post
$\mathbf{z}_i^*$
$\mathcal{S}_\theta$
f
ψ_θ^1
ψ_θ^2
ψ_θ^3
ψ_θ^4
Task Encoder $g_\theta(.)$
$g_\theta(\mathcal{S})$ or $g_\theta(\mathcal{S}, \mathcal{Q})$
ψ_θ

Figure 2: Overview of the neural adaptive feature extraction process used in Transductive/Simple CNAPS. Figure was adapted from Bateni et al. (2020).

(Liu et al., 2020) are two very recent methods that employ universal representations stemming from multiple domain-specific feature extraction heads. URT (Liu et al., 2020), which was developed and released publicly in parallel to this work, achieves state of the art performance by using a universal transformation layer.

2.2 Few-Shot Learning using Unlabelled Data

Several approaches (Kim et al., 2019; Liu et al., 2018; Ren et al., 2018) have also explored the use of unlabelled instances for few-shot visual classification. EGNN (Kim et al., 2019) employs a graph convolutional edge-labelling network for iterative propagation of labels from support to query instances. Similarly, TPN (Liu et al., 2018) learns a graph construction module for neural propagation of soft labels between elements of the query set. These methods rely on a neural parameterization of distance within the feature space. TEAM (Qiao et al., 2019) uses an episodic-wise transductive adaptable metric for performing inference on query examples using a task-specific metric. Song et al. (2020) use a cross attention network combined with a transductive iterative approach for augmenting the support set using the query examples. The closest method to our work is Ren et al. (2018). Their approach extends prototypical networks by performing a single additional soft-label weighted estimation of class prototypes. Our work, on the other hand, is different in three major ways. First, we produce soft-labelled estimates of both class mean and covariance. Second, we use an iterative algorithm with a data-driven convergence criterion allowing for a dynamic number of soft-label updates, depending on the task at hand. Lastly, we employ a neural adaptive procedure for feature extraction that is conditioned on a two-step learned transductive task representation, as opposed to a fixed feature-extractor. As we discuss in Section 4.2, this novel task-representation encoder is responsible for substantial performance gains on out-of-domain tasks.

3 Method

3.1 Problem Definition

Following (Snell et al., 2017; Bateni et al., 2020; Requeima et al., 2019; Finn et al., 2017), we focus on a few-shot classification setting where a distribution D over image classification tasks $(\mathcal{S}, \mathcal{Q})$ is provided for training. Each task $(\mathcal{S}, \mathcal{Q}) \sim D$ consists of a support set $\mathcal{S} = \{(\mathbf{x}_i, y_i)\}_{i=1}^n$ of labelled images and a query set $\mathcal{Q} = \{\mathbf{x}_i^*\}_{i=1}^m$ of unlabelled images; the goal is to predict labels for these query examples, given the (typically small) support set. Each query image $\mathbf{x}_i^* \in \mathcal{Q}$ has a corresponding ground truth label y_i^* available at training time. A model will be trained by minimizing, over some parameters θ (which are shared across tasks), the expected query set classification loss over tasks: $\mathbb{E}_{(\mathcal{S},\mathcal{Q})\sim D}[\sum_{\mathbf{x}_i^* \in \mathcal{Q}} - \log p_\theta(y_i^* | \mathbf{x}_i^*, \mathcal{S}, \mathcal{Q})]$; the inclusion of the dependence on all of $\mathcal{Q}$ here allows for the model to be transductive. At test time, a separate distribution of tasks generated from previously unseen images and classes is used to evaluate performance. We also define *shot* as the number of support examples per class, and *way* as the number of classes within the task.

3.2 Simple CNAPS

Our method extends the Simple CNAPS (Bateni et al., 2020) architecture for few-shot visual classification. Simple CNAPS performs few-shot classification in two steps. First, it computes task-adapted features for every support and query example. This part of the architecture is the same as that in CNAPS (Requeima et al., 2019), and is based on the FiLM metalearning framework (Perez et al.,

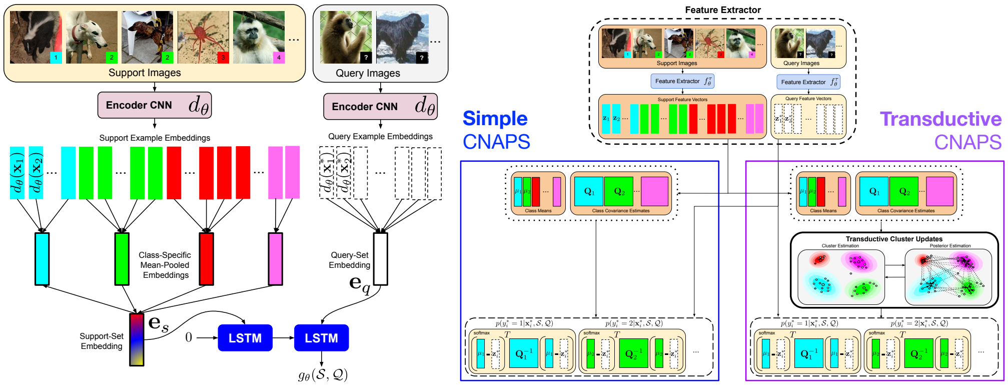

(a) Transductive Set-Encoder Overview

(b) Transductive CNAPS vs. Simple CNAPS

Figure 3: a) Overview of the transductive task-encoding procedure, $g_\theta(\mathcal{S}, \mathcal{Q})$, used in Transductive CNAPS. b) Transductive CNAPS (right) extends the Mahalanobis-distance based classifier in Simple CNAPS (left) through transductive soft k-means clustering of the visual space.

2018). Second, it uses the support set to estimate a per-class Mahalanobis metric, which is used to assign query examples to classes. The architecture uses a ResNet18 (He et al., 2015) feature extractor, which is pre-trained on some standard supervised dataset. Within each residual block, Feature-wise Linear Modulation (FiLM) layers compute a scale factor γ and shift β for each output channel, using block-specific adaptation networks ψ_θ that are conditioned on a task encoding. The task encoding $g_\theta(\mathcal{S})$ consists of the mean-pooled feature vectors of support examples produced by d_θ, a separate but end-to-end learned Convolution Neural Network (CNN). This produces an adapted feature extractor f_θ (which implicitly depends on the support set $\mathcal{S}$) that maps support/query images onto the corresponding adapted feature space. We will denote by $\mathcal{S}_\theta$, $\mathcal{Q}_\theta$ versions of the support/query sets where each image is mapped into its feature representation $\mathbf{z} = f_\theta(\mathbf{x})$. Simple CNAPS then computes a Mahalanobis distance relative to each class k by estimating a mean $\boldsymbol{\mu}_k$ and regularized covariance $\mathbf{Q}_k$ in the adapted feature space, using the support instances:

$$\boldsymbol{\mu}_k = \frac{1}{n_k} \sum_i \mathbb{I}[y_i = k]\, \mathbf{z}_i, \qquad \mathbf{Q}_k = \lambda_k\, \boldsymbol{\Sigma}_k + (1 - \lambda_k)\, \boldsymbol{\Sigma} + \beta I, \qquad \lambda_k = \frac{n_k}{n_k + 1}. \tag{1}$$

Here $\mathbb{I}[y_i = k]$ is the indicator function and $n_k = \sum_i \mathbb{I}[y_i = k]$ is the number of examples with class k in the support set $\mathcal{S}$. The ratio λ_k balances an task-conditional sample covariance $\boldsymbol{\Sigma}$ and a class-conditional sample covariance $\boldsymbol{\Sigma}_k$:

$$\boldsymbol{\Sigma} = \frac{1}{n} \sum_i \big(\mathbf{z}_i - \boldsymbol{\mu}\big)\big(\mathbf{z}_i - \boldsymbol{\mu}\big)^T, \qquad \boldsymbol{\Sigma}_k = \frac{1}{n_k} \sum_i \mathbb{I}[y_i = k]\, \big(\mathbf{z}_i - \boldsymbol{\mu}_k\big)\big(\mathbf{z}_i - \boldsymbol{\mu}_k\big)^T, \tag{2}$$

where $\boldsymbol{\mu} = \frac{1}{n} \sum_i \mathbf{z}_i$ is the task-level mean. When few support examples are available for a particular class, λ_k is small, and the estimate is regularized towards the task-level covariance $\boldsymbol{\Sigma}$. As the number of support examples for the class increases, the estimate tends to towards the class-conditional covariance $\boldsymbol{\Sigma}_k$. Additionally, an identity regularizer βI is added to the covariance estimate to ensure invertability of the covariance matrix. Given the class means and covariances, Simple CNAPS computes class probabilities for each query feature vector $\mathbf{z}^*_i$ through a softmax over the squared Mahalanobis distances with respect to each class:

$$p(y^* = k \mid \mathbf{z}^*) \propto \exp\big(-(\mathbf{z} - \boldsymbol{\mu}_k)^T \mathbf{Q}_k^{-1} (\mathbf{z} - \boldsymbol{\mu}_k)\big). \tag{3}$$

3.3 Transductive CNAPS

Transductive CNAPS extends Simple CNAPS by taking advantage of the query set, both in the feature adaptation step and the classification step. First, the task encoder g_θ is extended to incorporate both a support-set embedding $\mathbf{e}_s$ and a query-set embedding $\mathbf{e}_q$ such that,

$$\mathbf{e}_s = \frac{1}{K}\sum_k \frac{1}{n_k}\sum_i \mathbb{I}[y_i = k]\; d_\theta(\mathbf{x}_i), \qquad\qquad \mathbf{e}_q = \frac{1}{n_q}\sum_{i*} d_\theta(\mathbf{x}_i^*), \tag{4}$$

where d_θ is a learned CNN. The support embedding $\mathbf{e}_s$ is formed by an average of (encoded) support examples, with weighting inversely proportional to their class counts to prevent bias from class imbalance. The query embedding e_q uses simple mean-pooling; both $\mathbf{e}_s$ and $\mathbf{e}_q$ are invariant to permutations of the respective support/query instances. We then process e_s and e_q through two steps of a Long Short Term Memory (LSTM) network in the same order to generate the final transductive task-embedding $g_\theta(\mathcal{S}, \mathcal{Q})$ used for adaptation. This process is visualized in Figure 3-a.

Second, we can interpret Simple CNAPS as a form of supervised clustering in feature space; each cluster (corresponding to a class k) is parameterized with a centroid $\boldsymbol{\mu}_k$ and a metric $\mathbf{Q}_k^{-1}$, and we interpret equation 3 as class assignment probabilities based on the distance to each centroid. With this viewpoint in mind, a natural extension to consider is to use the estimates of the class assignment probabilities on unlabelled data to refine the class parameters $\boldsymbol{\mu}_k, \mathbf{Q}_k$ in a soft k-means framework based on per-cluster Mahalanobis distances (Melnykov & Melnykov, 2014). In this framework, as shown in Figure 1, we alternate between computing updated assignment probabilities using equation 3 on the query set and using those assignment probabilities to compute updated class parameters.

We will define $\mathcal{R}_\theta = \mathcal{S}_\theta \sqcup \mathcal{Q}_\theta$ as the disjoint union of the support set and the query set. For each element of $\mathcal{R}_\theta$, which we index by j, we define responsibilities w_{jk} in terms of their class predictions when it is part of the query set and in terms of the label when it is part of the support set,

$$w_{jk} = \begin{cases} p(y'_j = k \mid \mathbf{z}'_j) & \mathbf{z}'_j \in \mathcal{Q}_\theta, \\ \mathbb{I}[y'_j = k] & (\mathbf{z}'_j, y'_j) \in \mathcal{S}_\theta. \end{cases} \tag{5}$$

Using these responsibilities we can incorporate unlabelled samples from the support set by defining weighted estimates $\boldsymbol{\mu}'_k$ and $\mathbf{Q}'_k$:

$$\boldsymbol{\mu}'_k = \frac{1}{n'_k}\sum_j w_{jk}\,\mathbf{z}'_j \qquad\qquad \mathbf{Q}'_k = \lambda'_k \boldsymbol{\Sigma}'_k + (1 - \lambda'_k)\boldsymbol{\Sigma}' + \beta I, \tag{6}$$

where $n'_k = \sum_j w_{jk}$ defines $\lambda'_k = n'_k/(n'_k + 1)$, and the covariance estimates $\boldsymbol{\Sigma}'$ and $\boldsymbol{\Sigma}'_k$ are

$$\boldsymbol{\Sigma}' = \frac{1}{\sum_k n'_k}\sum_{jk} w_{jk}\big(\mathbf{z}'_j - \boldsymbol{\mu}'\big)\big(\mathbf{z}'_j - \boldsymbol{\mu}'\big)^T, \qquad \boldsymbol{\Sigma}'_k = \frac{1}{n'_k}\sum_j w_{jk}\big(\mathbf{z}'_j - \boldsymbol{\mu}'_k\big)\big(\mathbf{z}'_j - \boldsymbol{\mu}'_k\big)^T. \tag{7}$$

with $\boldsymbol{\mu}' = \left(\sum_k n'_k\right)^{-1}\sum_{jk} w_{jk}\mathbf{z}'_j$ being the task-level mean.

These update equations are simply weighted versions of the original Simple CNAPS estimators from Section 3.2, and reduce to them exactly in the case of an empty query set.

Algorithm 1 summarizes the soft k-means procedure based on these updates. We initialize our weights using only the labelled support set. We use those weights to compute class parameters, then compute updated weights using both the support and query sets. At this point, the weights associated with the query set $\mathcal{Q}$ are the same class probabilities as estimated by Simple CNAPS. However, we continue this procedure iteratively until we reach either reach a maximum number of iterations, or until class assignments $\text{argmax}_k\, w_{jk}$ stop changing.

Unlike the transductive task-encoder, this second extension, namely the soft k-mean iterative estimation of class parameters, is used at test time only. During training, a single estimation is produced for both mean and covariance using only the support examples. This, as we discuss more in Section 4.2, was shown to empirically perform better. See Figure 3-b for a high-level visual comparison of classification in Simple CNAPS vs. Transductive CNAPS.

4 Experiments

4.1 Benchmarks

Meta-Dataset (Triantafillou et al., 2019) is a few-shot image classification benchmark that consists of 10 widely used datasets: ILSVRC-2012 (ImageNet) (Russakovsky et al., 2015), Omniglot (Lake

Algorithm 1 Iterative Refinement in Transductive-CNAPS

```
procedure COMPUTE_QUERY_LABELS($\mathcal{S}_\theta, \mathcal{Q}_\theta, N_{\text{iter}}$)
    For $j$ ranging over support and query sets, $w_{jk} \leftarrow \begin{cases} 1 & \text{if } (\mathbf{z}'_j, y'_j) \in \mathcal{S}_\theta \text{ and } y_j = k \\ 0 & \text{otherwise} \end{cases}$
    for iter = $0 \cdots N_{\text{iter}}$ do        ▷ The first iteration is equivalent to Simple CNAPS;
        Compute class parameters $\boldsymbol{\mu}_k, \mathbf{Q}_k$ according to update equations equation 6-equation 7
        Compute class weights using class parameters according to equation 5
        break if the most probable class for each query example hasn't changed
    end for
    return class probabilities $w_{jk}$ for $j$ corresponding to $\mathcal{Q}_\theta$
end procedure
```

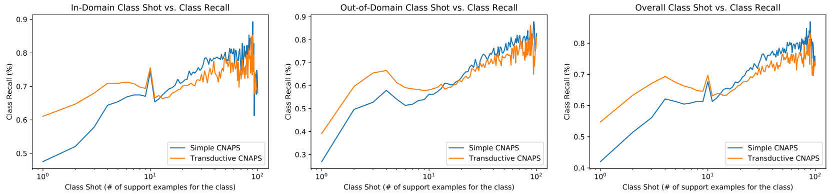

(a) In-Domain (b) Out-of-Domain (c) Overall

Figure 4: Class recall (otherwise noted as in-class query accuracy) averaged between classes across all tasks and (a: In-Domain, b: Out-of-domain, c: all) Meta-Dataset datasets. Class recalls have been grouped together, averaged and plotted according to the class shot in (a), (b), and (c).

et al., 2015), FGVC-Aircraft (Aircraft) (Maji et al., 2013), CUB-200-2011 (Birds) (Wah et al., 2011), Describable Textures (DTD) (Cimpoi et al., 2014), QuickDraw (Jongejan et al., 2016), FGVCx Fungi (Fungi) (Schroeder & Cui, 2018), VGG Flower (Flower) (Nilsback & Zisserman, 2008), Traffic Signs (Signs) (Houben et al., 2013) and MSCOCO (Lin et al., 2014). Consistent with past work (Requeima et al., 2019; Bateni et al., 2020), we train our model on the official training splits of the first 8 datasets and use the test splits to evaluate in-domain performance. We use the remaining two dataset as well as three external benchmarks, namely MNIST (LeCun & Cortes, 2010), CIFAR10 (Krizhevsky, 2009) and CIFAR100 (Krizhevsky, 2009), for out-of-domain evaluation. Task generation in Meta-Dataset follows a complex procedure where tasks can be of different *ways* and individual classes can be of varying *shots* even within the same task. Specifically, for each task, the task *way* is first sampled uniformly between 5 and 50 and *way* classes are selected at random from the corresponding class/dataset split. Then, for each class, 10 instances are sampled at random and used as query examples for the class, while of the remaining images for the class, a *shot* is sampled uniformly from [1, 100] and *shot* number of images are selected at random as support examples with total support set size of 500. Additional dataset-specific constraints are enforced, as discussed in Section 3.2 of (Triantafillou et al., 2019), and since some datasets have fewer than 50 classes and fewer than 100 images per class, the overall *way* and *shot* distributions resemble Poisson distributions where most tasks have fewer than 10 classes and most classes have fewer than 10 support examples (see Appendix-A.1). We train for a total of 110K tasks using Episodic Training (Snell et al., 2017; Finn et al., 2017) (see Appendix-A.3 for details).

mini/tiered-ImageNet (Vinyals et al., 2016; Ren et al., 2018) are two benchmarks for few-shot learning. Both datasets employ subsets of ImageNet (Russakovsky et al., 2015) with a total of 100 classes and 60K images in mini-ImageNet and 608 classes and 779K images in tiered-ImageNet. Unlike Meta-Dataset, tasks across these datasets have pre-defined *shots*/*ways* that are uniform across every task generated in the specified setting. Following (Nichol et al., 2018; Liu et al., 2018; Snell et al., 2017), we report performance on the 1/5-*shot* 5/10-*way* settings across both datasets with 10 query examples per class. We train episodically for 20K tasks (see Appendix-A.2 for details).

	In-Domain Accuracy (%)								Out-of-Domain Accuracy (%)					Avg Rank		
Model	ImageNet	Omniglot	Aircraft	Birds	DTD	QuickDraw	Fungi	Flower	Signs	MSCOCO	MNIST	CIFAR10	CIFAR100	In	Out	All
RelationNet	30.9±0.9	86.6±0.8	69.7±0.8	54.1±1.0	56.6±0.7	61.8±1.0	32.6±1.1	76.1±0.8	37.5±0.9	27.4±0.9	NA	NA	NA	10.5	11.0	10.6
MatchingNet	36.1±1.0	78.3±1.0	69.2±1.0	56.4±1.0	61.8±0.7	60.8±1.0	33.7±1.0	81.9±0.7	55.6±1.1	28.8±1.0	NA	NA	NA	10.1	8.5	9.8
MAML	37.8±1.0	83.9±1.0	76.4±0.7	62.4±1.1	64.1±0.8	59.7±1.1	33.5±1.1	79.9±0.8	42.9±1.3	29.4±1.1	NA	NA	NA	9.2	10.5	9.5
ProtoNet	44.5±1.1	79.6±1.1	71.1±0.9	67.0±1.0	65.2±0.8	64.9±0.9	40.3±1.1	86.9±0.7	46.5±1.0	39.9±1.1	NA	NA	NA	8.2	9.5	8.5
ProtoMAML	46.5±1.1	82.7±1.0	75.2±0.8	69.9±1.0	68.3±0.8	66.8±0.9	42.0±1.2	88.7±0.7	52.4±1.1	41.7±1.1	NA	NA	NA	7.1	8.0	7.3
CNAPS	52.3±1.0	88.4±0.7	80.5±0.6	72.2±0.9	58.3±0.7	72.5±0.8	47.4±1.0	86.0±0.5	60.2±0.9	42.6±1.1	92.7±0.4	61.5±0.7	50.1±1.0	6.6	6.0	6.4
BOHB-E	55.4±1.1	77.5±1.1	60.9±0.9	73.6±0.8	72.8±0.7	61.2±0.9	44.5±1.1	90.6±0.6	57.5±1.0	51.9±1.0	NA	NA	NA	6.4	4.0	5.9
TaskNorm	50.6±1.1	90.7±0.6	83.8±0.6	74.6±0.8	62.1±0.7	74.8±0.7	48.7±1.0	89.6±0.5	67.0±0.7	43.4±1.0	92.3±0.4	69.3±0.8	54.6±1.1	4.7	4.8	4.8
Simple CNAPS	**58.6±1.1**	91.7±0.6	82.4±0.7	74.9±0.8	67.8±0.8	77.7±0.7	46.9±1.0	90.7±0.5	73.5±0.7	46.2±1.1	93.9±0.4	74.3±0.7	60.5±1.0	3.4	3.0	3.2
SUR	56.3±1.1	93.1±0.5	**85.4±0.7**	71.4±1.0	**71.5±0.8**	81.3±0.6	**63.1±1.0**	82.8±0.7	70.4±0.8	**52.4±1.1**	94.3±0.4	66.8±0.9	56.6±1.0	3.1	2.6	2.9
URT	55.7±1.0	**94.4±0.4**	**85.8±0.6**	76.3±0.8	**71.8±0.7**	**82.5±0.6**	**63.5±1.0**	88.2±0.6	69.4±0.8	**52.2±1.1**	94.8±0.4	67.3±0.8	56.9±1.0	**1.7**	2.8	2.2
Our Method	**58.8±1.1**	**93.9±0.4**	84.1±0.6	**76.8±0.8**	69.0±0.8	78.6±0.7	48.8±1.1	**91.6±0.4**	**76.1±0.7**	48.7±1.0	**95.7±0.3**	**75.7±0.7**	**62.9±1.0**	2.1	**1.6**	**1.9**

Table 1: Few-shot classification on Meta-Dataset, MNIST, and CIFAR10/100. Error intervals showcase 95% confidence interval, and bold values indicate statistically significant state of the art performance. Average rank is obtained by ranking methods on each dataset and averaging the ranks.

		mini-ImageNet Accuracy (%)				tiered-ImageNet Accuracy (%)			
		5-*way*		10-*way*		5-*way*		10-*way*	
Model	Transductive	1-*shot*	5-*shot*	1-*shot*	5-*shot*	1-*shot*	5-*shot*	1-*shot*	5-*shot*
MAML (Finn et al., 2017)	BN	48.7±1.8	63.1±0.9	31.3±1.1	46.9±1.2	51.7±1.8	70.3±1.7	34.4±1.2	53.3±1.3
MAML+ (Liu et al., 2018)	Yes	50.8±1.8	66.2±1.8	31.8±0.4	48.2±1.3	53.2±1.8	70.8±1.8	34.8±1.2	54.7±1.3
Reptile (Nichol et al., 2018)	No	47.1±0.3	62.7±0.4	31.1±0.3	44.7±0.3	49.0±0.2	66.5±0.2	33.7±0.3	48.0±0.3
Reptile+BN (Nichol et al., 2018)	BN	49.9±0.3	66.0±0.6	32.0±0.3	47.6±0.3	52.4±0.2	71.0±0.2	35.3±0.3	52.0±0.3
ProtoNet (Snell et al., 2017)	No	46.1±0.8	65.8±0.7	32.9±0.5	49.3±0.4	48.6±0.9	69.6±0.7	37.3±0.6	57.8±0.5
RelationNet (Sung et al., 2018)	BN	51.4±0.8	67.0±0.7	34.9±0.5	47.9±0.4	54.5±0.9	71.3±0.8	36.3±0.6	58.0±0.6
TPN (Liu et al., 2018)	Yes	51.4±0.8	67.1±0.7	34.9±0.5	47.9±0.4	59.9±0.9	73.3±0.7	44.8±0.6	59.4±0.5
Transductive CNAPS (w CIFAR100)	Yes	53.5±1.0	73.3±0.8	35.0±0.5	58.7±0.5	52.2±1.0	72.2±0.9	34.3±0.6	59.0±0.6
AttWeightGen (Gidaris & Komodakis, 2018)	BN	56.2±0.9	73.0±0.6	NA	NA	NA	NA	NA	NA
TADAM (Oreshkin et al., 2018)	BN	58.5±0.3	76.7±0.3	NA	NA	NA	NA	NA	NA
LEO (Rusu et al., 2018)	BN	61.8±0.1	77.6±0.1	NA	NA	66.3±0.1	81.4±0.1	NA	NA
CNAPS (Requeima et al., 2019)	BN	77.8±1.0	87.6±0.7	65.7±0.7	80.0±0.6	75.7±1.0	85.5±0.7	63.7±0.7	78.2±0.5
Simple CNAPS (Bateni et al., 2020)	BN	80.5±0.9	89.5±0.6	68.6±0.7	83.7±0.5	79.0±0.9	87.6±0.6	67.1±0.7	81.0±0.5
Transductive CNAPS	Yes	**83.2±0.8**	**91.4±0.6**	**74.4±0.8**	**85.7±0.5**	**86.7±0.8**	**93.8±0.5**	**81.0±0.8**	**90.1±0.4**

Table 2: Few-shot visual classification results on 1/5-shot 5/10-way few-shot on mini/tiered-ImageNet. Unless otherwise noted, CNAPS-based models use a ResNet18 feature extractor pre-trained on Meta-Dataset's ImageNet training split. Error intervals showcase 95% confidence interval.

4.2 RESULTS

Evaluation on Meta-Dataset: In-domain, out-of-domain and overall rankings on Meta-Dataset are shown in Table 1. In this setting, we pre-train our ResNet feature extractor on the training split of the ImageNet subset of Meta-Dataset. Transductive CNAPS sets new state of the art accuracy on 2 out of the 8 in-domain datasets, while matching other methods on 2 of the remaining domains. On out-of-domain tasks, it performs better with new state of the art performance on 4 out of the 5 ou-of-domain datasets, Overall, it produces an average rank of 1.9 among all datasets, the best among the methods, with an average rank of 2.1 on in-domain tasks, only second to URT which was developed parallel to Transductive CNAPS, and 1.6 on out-of-domain tasks, the best among even the most recent methods.

Evaluation on mini/tiered-ImageNet: As shown in Table 2, when the ResNet18 feature extractor is pre-trained on a rich dataset (the training split of the ImageNet subset of Meta-Dataset), we outperform all other baselines. We emphasize, however, that due to a substantial amount of data overlap between the training split of Meta-Dataset's ImageNet and the mini-/tiered-ImageNet test split, we can only directly compare these results to other CNAPS-based models; this provides a window into the gains we are getting from transduction, but does not help us compare to other transductive approaches. To address this, we have excluded the overlapping classes from the ResNet18 pre-training set, and are in the process of re-training the feature extractor. Due to our training resources, these results have not been completed in time for submission. In lieu of this, we have provided results with a feature extractor pre-trained on CIFAR100. With this feature extractor, we achieve competitive (but not state of the art) performance when compared to many transductive baselines. We expect these CIFAR100-based results to act as a lower bound for the performance that we will see with the updated ImageNet-trained ResNet.

	In-Domain Accuracy (%)								Out-of-Domain Accuracy (%)					Avg Acc.		
CNAPS Model	ImageNet	Omniglot	Aircraft	Birds	DTD	QuickDraw	Fungi	Flower	Signs	MSCOCO	MNIST	CIFAR10	CIFAR100	In	Out	All
GMM-EM+	53.3±1.0	91.8±0.6	81.2±0.6	**75.8±0.7**	**71.8±0.6**	72.9±0.7	42.8±0.9	91.0±0.4	66.1±0.8	40.3±1.0	94.2±0.4	69.0±0.7	51.3±0.9	72.6	64.2	69.3
GMM	45.3±1.0	88.0±0.9	80.8±0.8	71.4±0.8	61.1±0.7	70.7±0.8	42.9±1.0	88.1±0.6	68.9±0.7	37.2±0.9	91.4±0.5	64.5±0.7	46.6±0.9	68.5	61.7	65.9
FEOT GMM	52.6±1.1	89.6±0.7	**84.0±0.6**	76.2±0.8	66.5±0.8	73.4±0.8	45.7±1.0	89.8±0.6	74.4±0.7	44.2±1.0	93.1±0.4	71.1±0.8	56.9±1.0	72.2	67.9	70.6
COT GMM	48.7±1.0	92.3±0.5	80.0±0.7	72.4±0.7	59.8±0.7	71.1±0.7	41.4±0.9	87.7±0.5	63.6±0.8	39.2±0.8	89.8±0.5	66.9±0.7	50.5±0.8	69.2	62.0	66.4
GMM-EM	52.3±1.0	92.0±0.5	**84.3±0.6**	75.2±0.8	64.3±0.7	72.6±0.8	44.6±1.0	90.8±0.5	71.4±0.7	44.7±0.9	93.0±0.4	71.1±0.7	56.4±0.9	72.0	67.3	70.2
Transductive+	53.3±1.1	92.3±0.5	81.2±0.7	75.0±0.8	**72.0±0.7**	74.8±0.8	45.1±1.0	92.1±0.4	71.0±0.8	44.0±1.1	95.9±0.3	71.1±0.7	57.3±1.1	73.2	67.9	71.2
Simple	**58.6±1.1**	91.7±0.6	82.4±0.7	74.9±0.8	67.8±0.8	77.7±0.7	46.9±1.0	90.7±0.5	73.5±0.7	46.2±1.1	93.9±0.4	74.3±0.7	60.5±1.0	73.8	69.7	72.2
FEOT	**57.3±1.1**	90.5±0.7	82.9±0.7	74.8±0.8	67.3±0.8	76.3±0.8	47.7±1.0	90.5±0.5	**75.8±0.7**	**47.1±1.1**	94.9±0.4	74.3±0.8	**61.2±1.0**	73.4	70.7	72.4
COT	**58.8±1.1**	**95.2±0.3**	**84.0±0.6**	**76.4±0.7**	68.5±0.8	**77.8±0.7**	**49.7±1.0**	**92.7±0.4**	70.8±0.7	**47.3±1.0**	94.2±0.4	**75.2±0.7**	**61.2±1.0**	**75.4**	69.7	**73.2**
Transductive	**58.8±1.1**	93.9±0.4	**84.1±0.6**	**76.8±0.8**	69.0±0.8	**78.6±0.7**	**48.8±1.1**	91.6±0.4	**76.1±0.7**	**48.7±1.0**	**95.7±0.3**	**75.7±0.7**	**62.9±1.0**	**75.2**	**71.8**	**73.9**

Table 3: Performance of various ablations of Tranductive and Simple CNAPS on Meta-Dataset. Error intervals showcase 95% confidence interval, and bold values indicate statistically significant state of the art performance.

Performance vs. Class Shot: In Figure 4, we examine the relationship between class recall (i.e. accuracy among query examples belonging to the class itself) and the number of support examples in the class (shot). As shown, Transductive CNAPS is very effective when class shot is below 10, showing large average recall improvements, especially at the 1-shot level. However, as the class shot increases beyond 10, performance drops compared to Simple CNAPS. This suggests that soft k-means learning of cluster parameters can be effective when very few support examples are available. Conversely, in high-shot classes, transductive updates can act as distractors.

Training with Classification-Time Soft K-means Clustering: In our work, we use soft k-means iterative updates of means and covariance at test-time only. It's natural to consider training the feature adaptation network end-to-end through the soft k-means transduction procedure. We provide this comparison in the bottom-half of Table 3, with "Transductive+ CNAPS" denoting this variation. Iterative updates during training result in an average accuracy decrease of 2.5%, which we conjecture to be due to training instabilities caused by applying this iterative algorithm early in training on noisy features.

Transductive Feature Extraction vs. Classification: Our approach extends Simple CNAPS in two ways: improved adaptation of the feature extractor using a transductive task-encoding, and the soft k-means iterative estimation of class means and covariances. We perform two ablations, "Feature Extraction Only Transductive" (FEOT) and "Classification Only Transductive" (COT), to independently assess the impact of these extensions. The results are presented in Table 3. As shown, both extensions outperform Simple CNAPS. The transductive task-encoding is especially effective on out-of-domain tasks whereas the soft k-mean learning of class parameters boosts accuracy on in-domain tasks. Transductive CNAPS is able to leverage the best of both worlds, allowing it to achieve statistically significant gains over Simple CNAPS overall.

Comparison to Gaussian Mixture Models: The Mahalanobis-distance based class probabilities produced by Equation 3 closely resembles the cluster posterior probabilities (responsibilities) inferred by a Gaussian Mixture Model (GMM). The only changes required to make this correspondence exact is to introduce a class prior distribution π, and to change the class probability model equation 3 to the Gaussian likelihood:

$$p(y^* = k \mid \mathbf{z}^*) \propto \pi(y^* = k) \exp\left(-\frac{1}{2}(\mathbf{z} - \boldsymbol{\mu_k})^T \mathbf{Q}_k^{-1}(\mathbf{z} - \boldsymbol{\mu}_k) - \frac{1}{2}\log|\mathbf{Q}_k|\right) \tag{8}$$

With these modifications, Transductive CNAPS would exactly correspond to inference in a GMM, with cluster parameters learned through semi-supervised expectation maximization (EM). Given this observation, we consider five GMM-based ablations of our method where the log-determinant is introduced (a uniform class prior is used). These ablations are presented in Table 3 and correspond to their soft k-means counterparts in the same order shown. The GMM-based variations of our method and Simple CNAPS result in a notable 4-8% loss in overall accuracy. It's also surprising to observe that the FEOT variation matches the performance of the full GMM-EM model.

5 Discussion

In this paper, we have presented a few-shot visual classification method that achieves new state of the art performance via a transductive clustering procedure for refining class parameters derived from a previous neural adaptive Mahalanobis-distance based approach. The resulting architecture, Transductive CNAPS, is more effective at producing useful estimates of class mean and covariance especially in low-shot settings, when used at test time. Even though we demonstrate the efficacy of our approach in the transductive domain where query examples themselves are used as unlabelled data, our soft k-means clustering procedure can naturally extend to use other sources of unlabelled examples in a semi-supervised fashion.

Transductive CNAPS superficially resembles a transductive GMM model stacked on top of a learned feature representation; however, when we try to make this connection exact (by including the log-determinant of the class covariances), we suffer substantial performance hits. Explaining why this happens will be the subject of future work.

References

Peyman Bateni, Raghav Goyal, Vaden Masrani, Frank Wood, and Leonid Sigal. Improved few-shot visual classification. In *Proceedings of the IEEE/CVF Conference on Computer Vision and Pattern Recognition (CVPR)*, June 2020.

Aurélien Bellet, Amaury Habrard, and Marc Sebban. A survey on metric learning for feature vectors and structured data. *arXiv preprint arXiv:1306.6709*, 2013.

Mircea Cimpoi, Subhransu Maji, Iasonas Kokkinos, Sammy Mohamed, and Andrea Vedaldi. Describing textures in the wild. In *Proceedings of the IEEE Conference on Computer Vision and Pattern Recognition*, pp. 3606–3613, 2014.

Nikita Dvornik, Cordelia Schmid, and Julien Mairal. Selecting relevant features from a multi-domain representation for few-shot classification, 2020.

Abdur R Feyjie, Reza Azad, Marco Pedersoli, Claude Kauffman, Ismail Ben Ayed, and Jose Dolz. Semi-supervised few-shot learning for medical image segmentation, 2020.

Chelsea Finn, Pieter Abbeel, and Sergey Levine. Model-agnostic meta-learning for fast adaptation of deep networks. In *Proceedings of the 34th International Conference on Machine Learning-Volume 70*, pp. 1126–1135. JMLR. org, 2017.

Marta Garnelo, Dan Rosenbaum, Chris J. Maddison, Tiago Ramalho, David Saxton, Murray Shanahan, Yee Whye Teh, Danilo J. Rezende, and S. M. Ali Eslami. Conditional neural processes. *CoRR*, abs/1807.01613, 2018. URL `http://arxiv.org/abs/1807.01613`.

Spyros Gidaris and Nikos Komodakis. Dynamic few-shot visual learning without forgetting. *CoRR*, abs/1804.09458, 2018. URL `http://arxiv.org/abs/1804.09458`.

Kaiming He, Xiangyu Zhang, Shaoqing Ren, and Jian Sun. Deep residual learning for image recognition. *CoRR*, abs/1512.03385, 2015. URL `http://arxiv.org/abs/1512.03385`.

Sebastian Houben, Johannes Stallkamp, Jan Salmen, Marc Schlipsing, and Christian Igel. Detection of traffic signs in real-world images: The german traffic sign detection benchmark. In *The 2013 international joint conference on neural networks (IJCNN)*, pp. 1–8. IEEE, 2013.

Jonas Jongejan, Henry Rowley, Takashi Kawashima, Jongmin Kim, and Nick Fox-Gieg. The quick, draw!-ai experiment.(2016), 2016.

Jongmin Kim, Taesup Kim, Sungwoong Kim, and Chang D. Yoo. Edge-labeling graph neural network for few-shot learning. *CoRR*, abs/1905.01436, 2019. URL `http://arxiv.org/abs/1905.01436`.

Gregory Koch, Richard Zemel, and Ruslan Salakhutdinov. Siamese neural networks for one-shot image recognition. In *ICML deep learning workshop*, volume 2, 2015.

Alex Krizhevsky. Learning multiple layers of features from tiny images. Technical report, 2009.

Alex Krizhevsky, Ilya Sutskever, and Geoffrey E. Hinton. Imagenet classification with deep convolutional neural networks. *Commun. ACM*, 60(6):84–90, May 2017. ISSN 0001-0782. doi: 10.1145/3065386. URL `http://doi.acm.org/10.1145/3065386`.

Brenden M Lake, Ruslan Salakhutdinov, and Joshua B Tenenbaum. Human-level concept learning through probabilistic program induction. *Science*, 350(6266):1332–1338, 2015.

Yann LeCun and Corinna Cortes. MNIST handwritten digit database. 2010. URL `http://yann.lecun.com/exdb/mnist/`.

Tsung-Yi Lin, Michael Maire, Serge Belongie, James Hays, Pietro Perona, Deva Ramanan, Piotr Dollár, and C Lawrence Zitnick. Microsoft coco: Common objects in context. In *European conference on computer vision*, pp. 740–755. Springer, 2014.

Lu Liu, William Hamilton, Guodong Long, Jing Jiang, and Hugo Larochelle. A universal representation transformer layer for few-shot image classification, 2020.

Yanbin Liu, Juho Lee, Minseop Park, Saehoon Kim, and Yi Yang. Transductive propagation network for few-shot learning. *CoRR*, abs/1805.10002, 2018. URL `http://arxiv.org/abs/1805.10002`.

Subhransu Maji, Esa Rahtu, Juho Kannala, Matthew Blaschko, and Andrea Vedaldi. Fine-grained visual classification of aircraft. *arXiv preprint arXiv:1306.5151*, 2013.

Igor Melnykov and Volodymyr Melnykov. On k-means algorithm with the use of mahalanobis distances. *Statistics & Probability Letters*, 84:88–95, 2014.

Nikhil Mishra, Mostafa Rohaninejad, Xi Chen, and Pieter Abbeel. Meta-learning with temporal convolutions. *CoRR*, abs/1707.03141, 2017. URL `http://arxiv.org/abs/1707.03141`.

Alex Nichol, Joshua Achiam, and John Schulman. On first-order meta-learning algorithms. *CoRR*, abs/1803.02999, 2018. URL `http://arxiv.org/abs/1803.02999`.

Maria-Elena Nilsback and Andrew Zisserman. Automated flower classification over a large number of classes. In *2008 Sixth Indian Conference on Computer Vision, Graphics & Image Processing*, pp. 722–729. IEEE, 2008.

Boris Oreshkin, Pau Rodríguez López, and Alexandre Lacoste. Tadam: Task dependent adaptive metric for improved few-shot learning. In S. Bengio, H. Wallach, H. Larochelle, K. Grauman, N. Cesa-Bianchi, and R. Garnett (eds.), *Advances in Neural Information Processing Systems 31*, pp. 721–731. Curran Associates, Inc., 2018. URL `http://papers.nips.cc/paper/7352-tadam-task-dependent-adaptive-metric-for-improved-few-shot-learning.pdf`.

Ethan Perez, Florian Strub, Harm De Vries, Vincent Dumoulin, and Aaron Courville. Film: Visual reasoning with a general conditioning layer. In *Thirty-Second AAAI Conference on Artificial Intelligence*, 2018.

Limeng Qiao, Yemin Shi, Jia Li, Yaowei Wang, Tiejun Huang, and Yonghong Tian. Transductive episodic-wise adaptive metric for few-shot learning. In *Proceedings of the IEEE/CVF International Conference on Computer Vision (ICCV)*, October 2019.

Sachin Ravi and Hugo Larochelle. Optimization as a model for few-shot learning. In *5th International Conference on Learning Representations, ICLR 2017, Toulon, France, April 24-26, 2017, Conference Track Proceedings*, 2017. URL `https://openreview.net/forum?id=rJY0-Kcll`.

Mengye Ren, Eleni Triantafillou, Sachin Ravi, Jake Snell, Kevin Swersky, Joshua B. Tenenbaum, Hugo Larochelle, and Richard S. Zemel. Meta-learning for semi-supervised few-shot classification. *CoRR*, abs/1803.00676, 2018. URL `http://arxiv.org/abs/1803.00676`.

James Requeima, Jonathan Gordon, John Bronskill, Sebastian Nowozin, and Richard E Turner. Fast and flexible multi-task classification using conditional neural adaptive processes. *arXiv preprint arXiv:1906.07697*, 2019.

Olga Russakovsky, Jia Deng, Hao Su, Jonathan Krause, Sanjeev Satheesh, Sean Ma, Zhiheng Huang, Andrej Karpathy, Aditya Khosla, Michael Bernstein, et al. Imagenet large scale visual recognition challenge. *International journal of computer vision*, 115(3):211–252, 2015.

Andrei A. Rusu, Dushyant Rao, Jakub Sygnowski, Oriol Vinyals, Razvan Pascanu, Simon Osindero, and Raia Hadsell. Meta-learning with latent embedding optimization. *CoRR*, abs/1807.05960, 2018. URL `http://arxiv.org/abs/1807.05960`.

Victor Garcia Satorras and Joan Bruna Estrach. Few-shot learning with graph neural networks. In *International Conference on Learning Representations*, 2018. URL `https://openreview.net/forum?id=BJj6qGbRW`.

B. Schroeder and Y Cui. Fgvcx fungi classification challenge 2018. `https://github.com/visipedia/fgvcx_fungi_comp`, 2018.

Karen Simonyan and Andrew Zisserman. Very deep convolutional networks for large-scale image recognition. *arXiv 1409.1556*, 09 2014.

Jake Snell, Kevin Swersky, and Richard Zemel. Prototypical networks for few-shot learning. In *Advances in Neural Information Processing Systems*, pp. 4077–4087, 2017.

Xibin Song, Yuchao Dai, Dingfu Zhou, Liu Liu, Wei Li, Hongdong Li, and Ruigang Yang. Channel attention based iterative residual learning for depth map super-resolution. In *IEEE/CVF Conference on Computer Vision and Pattern Recognition (CVPR)*, June 2020.

M. Sornam, K. Muthusubash, and V. Vanitha. A survey on image classification and activity recognition using deep convolutional neural network architecture. In *2017 Ninth International Conference on Advanced Computing (ICoAC)*, pp. 121–126, Dec 2017. doi: 10.1109/ICoAC.2017.8441512.

Flood Sung, Yongxin Yang, Li Zhang, Tao Xiang, Philip HS Torr, and Timothy M Hospedales. Learning to compare: Relation network for few-shot learning. In *Proceedings of the IEEE Conference on Computer Vision and Pattern Recognition*, pp. 1199–1208, 2018.

Christian Szegedy, Wei Liu, Yangqing Jia, Pierre Sermanet, Scott E. Reed, Dragomir Anguelov, Dumitru Erhan, Vincent Vanhoucke, and Andrew Rabinovich. Going deeper with convolutions. *CoRR*, abs/1409.4842, 2014. URL `http://arxiv.org/abs/1409.4842`.

Eleni Triantafillou, Tyler Zhu, Vincent Dumoulin, Pascal Lamblin, Kelvin Xu, Ross Goroshin, Carles Gelada, Kevin Swersky, Pierre-Antoine Manzagol, and Hugo Larochelle. Meta-dataset: A dataset of datasets for learning to learn from few examples. *arXiv preprint arXiv:1903.03096*, 2019.

Oriol Vinyals, Charles Blundell, Timothy Lillicrap, Daan Wierstra, et al. Matching networks for one shot learning. In *Advances in neural information processing systems*, pp. 3630–3638, 2016.

Catherine Wah, Steve Branson, Peter Welinder, Pietro Perona, and Serge Belongie. The caltech-ucsd birds-200-2011 dataset. 2011.

Wei Wang, Vincent W. Zheng, Han Yu, and Chunyan Miao. A survey of zero-shot learning: Settings, methods, and applications. *ACM Trans. Intell. Syst. Technol.*, 10(2):13:1–13:37, January 2019. ISSN 2157-6904. doi: 10.1145/3293318. URL `http://doi.acm.org/10.1145/3293318`.

Yaqing Wang and Quanming Yao. Few-shot learning: A survey. *CoRR*, abs/1904.05046, 2019. URL `http://arxiv.org/abs/1904.05046`.

Jason Yosinski, Jeff Clune, Yoshua Bengio, and Hod Lipson. How transferable are features in deep neural networks? *CoRR*, abs/1411.1792, 2014. URL `http://arxiv.org/abs/1411.1792`.

A Benchmarks and Training

A.1 Meta-Dataset

A brief description of the sampling procedure used in the Meta-Dataset setting is already provided in Section 4.1. This sampling procedure, however, comes with additional specifications that are uniform across all tasks (such as count enforcing) and dataset specific details such as considering the class hierarchy in ImageNet tasks. The full algorithm for sampling is outlined in (Triantafillou et al., 2019), and we refer the interested reader to Section 3.2 in (Triantafillou et al., 2019) for complete details. This procedure results in a task distribution where most tasks have fewer than 10 classes and each class has fewer than 20 support examples. The task frequency relative to the number of classes is presented in Figure 5a, and the class frequency as compared to the class shot is presented in Figure 5b. The query set contains between 1 and 10 (inclusive) examples per class for all tasks; fewer than 10 query examples occur only when there are not enough total images to support 10 query examples.

A.2 mini/tiered-ImageNet

Task sampling across both mini-ImageNet and tiered-ImageNet first starts by defining a constant number of ways and shots that will be used for each generated task. For a L-shot K-way problem setting, first K classes are sampled from the dataset with random probability. Then, for each sampled class, L of the class images are sampled with random probability and used as the support examples for the class. In addition, 10 query images (distinct from the support images) are sampled per class.

A.3 Meta-Dataset Training/Testing

Following (Bateni et al., 2020; Requeima et al., 2019), we train using Episodic training (Snell et al., 2017; Finn et al., 2017) where tasks themselves are used as training examples. For each iteration of Episodic training, a task (with additional ground truth query labels is generated, and the adaptation network is trained to minimize the classification error (cross entropy) of the query set given the task. The pre-trained ResNet18 feature extractor is fixed during this process. We train for a total of 110K tasks, with 16 tasks per batch, resulting in 6875 gradient updates. We train using Adam optimizer with learning rate of 5×10^{-4}. We evaluate on the validation splits of all 8 in-domain and 1 out-of-domain (MSCOCO) datasets, saving the best performing checkpoint for test-time evaluation.

A.4 mini/tiered-ImageNet Training/Testing

Similar to Meta-Dataset, we use Episodic training: at each iteration, a task is generated, and we backpropagate the query set classification loss through the adaptation network. For mini/tiered-ImageNet, we train for a total of 20K tasks, validating performance every 2K tasks and saving the best checkpoint for test-time evaluation. We, similarly, use the Adam optimiser with learning rate of 5×10^{-4}, and use a batch size of 16, for a total of 1250 gradient steps.

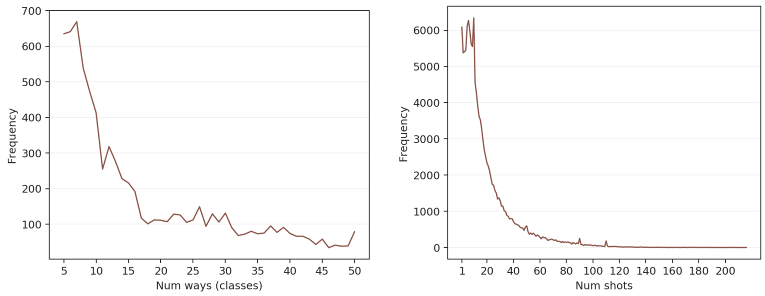

(a) Number of Tasks vs. Ways

(b) Number of Classes vs. Shots

Figure 5: Test-time way and shot frequency graphs. Figure is directly from (Bateni et al., 2020). As shown, most tasks have fewer than 10 classes (way) and most classes have less than 20 support examples (shot).